Journal of the European Ceramic Society 7 (1991) 249–254

Effect of Flaw–Flaw Interaction on the Strength of a Soda-Lime Glass

M. Sakai & T. Miyajima

Department of Materials Science, Toyohashi University of Technology, Tempaku-cho, Toyohashi 441, Japan

(Received 26 September 1990; accepted 16 November 1990)

Abstract

The interaction between microflaws in ceramics is investigated through model fracture tests using soda-lime glass bend bars. A strength plateau arises through the microscopic transition of the fracture origin from the strength-controlling flaw to the model inherent flaw. A phenomenological expression is proposed which unifies the strength versus flaw size relationship over a wide range of flaw dimensions. The expression used the concept of the transition of the fracture origin, where the interaction of the strength-controlling flaw with intrinsic flaws was taken into account by the interaction function, $I(c/c_0)$.

Die Wechselwirkung zwischen Mikrorissen in keramischen Materialien wurde anhand modellhafter Festigkeitsmessungen an Biegebruchproben aus einem Na–Ca-Silikatglas untersucht. Bei steter Verkleinerung des festigkeitskontrollierenden Fehlers dominieren nach einem Übergangsbereich interne Fehler, was zu konstanten Festigkeitswerten (Festigkeitsplateau) führt. Es wird eine phänomenologische Gleichung vorgeschlagen, die den Zusammenhang zwischen der Festigkeit und der Fehlergröße vereinheitlicht und über einen weiten Fehlergrößenbereich beschreibt. Die Gleichung bezieht den Übergangsbereich insofern mit ein, als daß die Wechselwirkung des festigkeitskontrollierenden Fehlers mit inneren Fehlern durch die Wechselwirkungsfunktion $I(c/c_0)$ berücksichtigt wurde.

On a étudié l'interaction entre micro-défauts dans les céramiques à l'aide d'essais modélisés de rupture sur des éprouvettes de flexion en verre de chaux sodée. On observe un palier de résistance mécanique qui provient de la modification microscopique de l'origine de la rupture, passant d'un défaut contrôlant la rupture à un défaut inhérent au modèle. On propose une expression phénoménologique généralisant la relation exprimant la résistance mécanique en fonction de la taille du défaut, couvrant une gamme étendue de taille de défauts. Dans cette expression, on utilise le concept de modification de l'origine de la rupture, pour lequel l'interaction des défauts contrôlant la rupture avec les défauts intrinsèques est prise en compte par la fonction d'interaction, $I(c/c_0)$.

1 Introduction

In structural ceramics, strengths of 500 to 1500 MPa are generally required for practical uses as engineering components. This requirement implies that the dimension of the strength-controlling flaws ranges from 10 to 60 μm, assuming a fracture toughness (K_{Ic}) of about 5 MPam$^{1/2}$. From a microstructural viewpoint this flaw size is on the same order of magnitude as the sintered ceramic grain size. Thus, the assumption of the uniformity and continuity of the body in the linear elastic fracture mechanics regime will not hold, since the strength-controlling microflaw might be surrounded by ceramic grains with similar dimensions. Therefore, the fracture toughness (K_c(micro)) which dictates the critical stress level of crack initiation for such small flaws will have a different physical meaning and value than the fracture toughness (K_c(macro)) determined by the conventional fracture mechanics specimens which imply macroflaws, such as notches and precracks. In fact, the fractographic studies of Rice and coworkers[1,2] demonstrated that there is a tendency associated with the decrease in the flaw size for the measured fracture toughness to be less than

Journal of the European Ceramic Society 0955-2219/91/$3.50

the expected macroscopic toughness values (K_c(macro)). The study concluded that the toughness is determined by single-crystal cleavage energy or grain-boundary energy at the lower end of the crack size. This energy is averaged out over the ceramic microstructure at larger crack sizes to yield the polycrystalline toughness value.

Cook and coworkers[3] have made a study on the strength characteristics using controlled Vickers indentation flaws in several polycrystalline ceramics. With progressively diminishing indentation load (P), they observed a steady increase in strength followed by a strength plateau as the indentation load approached its characteristic load (P^*). To describe this scale transition, they extended the conventional indentation fracture mechanics to account for the microstructural effect. The resulting expression for the microstructural R-curve behavior,

$$K_c^{app}(P)/K_c(\text{macro}) = [P/(P + P^*)]^{1/4}$$

signifies the steady decrease in apparent toughness ($K_c^{app}(P)$) with diminishing indentation-induced flaw size. A similar study addressing such unusual decreases in K_c^{app} with diminishing flaw size was also conducted by Usami and coworkers.[4]

Upon considering the fracture processes of strength-controlling microflaws which are surrounded by ceramic grains with similar dimensions, their microstructural interactions with ceramic grain boundaries, intrinsic defects, micro-inclusions, pores, etc., may dominate the stress–strain field around these microflaws. The micromechanics details of microstructural R-curve behavior must be described completely in terms of this microstructural interaction as well as the nonlinear processes (grain bridging, martensitic phase-transformation, etc.) which may occur in the process zone wake region of propagating cracks and flaws. However, the studies on the interaction have always been hampered by the extreme difficulties in characterizing and controlling the microstructures of real polycrystalline ceramics.

A model fracture system was developed in the present work to minimize the above-mentioned difficulties, in which both of the strength-controlling microflaw (c) and the model inherent flaw (c_0) were quantitatively generated by indentation technique on the defect-free surfaces of float glass with three-point bend bar geometry. Because of its complete homogeneity and the uniformity over the μm-region of glass, it is possible to make unambiguous conclusions about the interaction between those model flaws.

2 Experimental

2.1 Material and fracture specimen

Bend bar specimens (4·8 × 5 × 60 mm) were machined from soda-lime float glass plates (4·8 mm thick, Nihon Plate Glass Co. Ltd). The edges of the bend specimens were chamfered and polished with 0·05-μm Al_2O_3 abrasives. Controlled flaws were introduced on the defect-free 'virgin' surface (i.e., the side which had not contacted the molten tin surface during the glass-making process). Three different types of model flaw geometries were generated as illustrated in Fig. 1: the reference model (Fig. 1(a)), the model without microstructural interaction which is termed 'non-interacting model' (Fig. 1(b)), and the 'interacting model' (Fig. 1(c)). The reference model has only a central surface flaw (c) and hence no influence from the model inherent flaws. For the non-interacting and the interacting models, two of the model inherent flaws with identical size (c_0) were introduced symmetrically in the center of the tension surface of the flexural specimen by a constant indentation load (P_0) of 4·9 N (=500 gf) using a standard Vickers hardness tester. The spacing between these controlled flaws ($2r$) was 600 μm for the non-interacting model, and 300 μm for the interacting model. A central flaw (c) was indented between these two model inherent flaws using different indentation load (P) ranging from 0·2 N to 50 N. Thus the microstructural interaction between c and c_0 could be examined by changing the relative flaw size (c) and by controlling the extent of the fracture mechanics interaction between c and c_0.

Following the indentations, the specimens were placed in distilled water at room temperature for 24 h to minimize the indentation-induced contact residual stresses. The specimens were then cleaned with acetone and held in a desiccator with silica gel for at least one week.

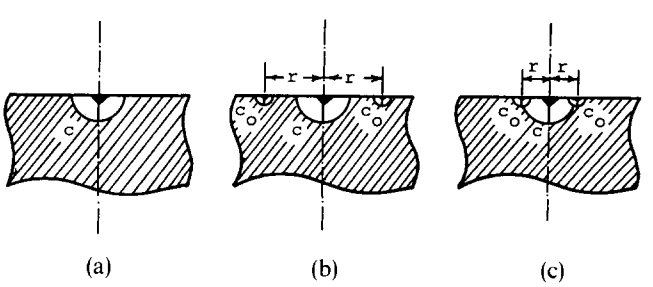

Fig. 1. Model surface flaws generated on the tension surface of flexural specimens. c and c_0 are strength-controlling central flaw and inherent model flaws, respectively. (a) Reference model; (b) non-interacting model (r = 300 μm); (c) interacting model (r = 150 μm).

2.2 Flexural test

The three-point flexural tests were conducted over a loading span of 50 mm with the specimens immersed in dry silicone oil (KF96 (100 centipoise), Sin-etsu Chemical Co. Ltd), to prevent the stress corrosion cracking. The displacement-controlled test machine was operated at a crosshead speed of 0·5 mm/min (about 5 MPa/s). The surface lengths ($2c$ and $2c_0$) of the controlled flaws (radial cracks) were optically measured on the indented surface.

The strength (σ) and the apparent fracture toughness (K_c^{app}) were, respectively, calculated by[5]

$$\sigma = 3FS/2BW^2 \quad (1)$$

and[6]

$$K_c^{app} = 0{\cdot}64\,.\,\sigma\,.\,(\pi c)^{1/2} \quad (2)$$

where F is the flexural load at failure, and S, B and W are the loading span (50·0 mm), thickness (5·0 mm) and the width (4·8 mm) of the flexural specimen, respectively.

3 Results

The flexural strengths (σ) for the non-interacting model and the reference model are plotted against indentation load (P) in Fig. 2. It is clear that a sharp transition in strength occurs at $P = P_0$ ($=4{\cdot}9$ N; the indentation load for generating the model inherent flaws (c_0)). The strengths (σ) of the non-interacting model specimens for $P > P_0$, and of the reference model specimens over all the indentation loads, are apparently determined by the central flaw (c). The slope of the straight line in Fig. 2 is 1/3. In the region

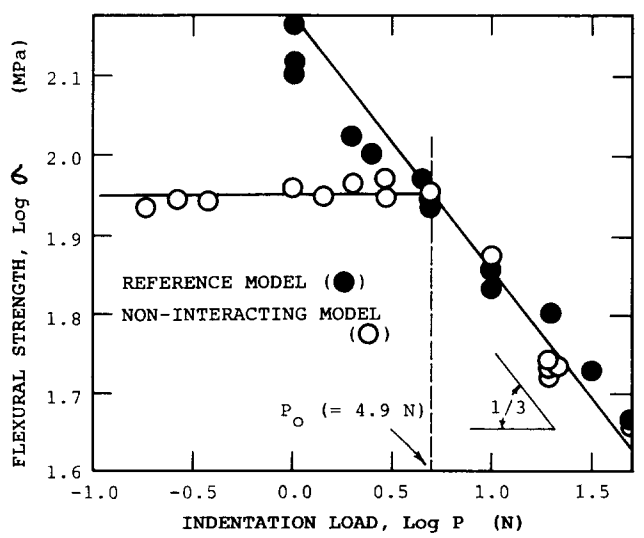

Fig. 2. Flexural strength of the reference model (●) and the non-interacting model (○) as a function of Vickers indentation load.

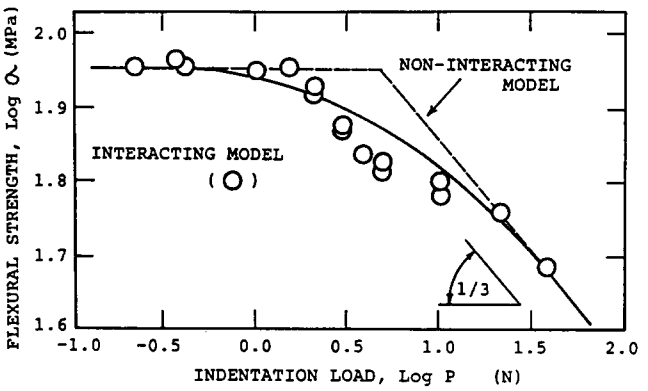

Fig. 3. Dependence of the flexural strength of the interacting model on the Vickers indentation load. Dashed lines are for the non-interacting model plotted in Fig. 2.

of $P < P_0$, the strength of the non-interacting model is independent of indentation load. The plateau strength (σ_0) is controlled by the model inherent flaw, c_0, and suggests a sharp transition of the fracture origin from c to c_0 at $P = P_0$.

The strength versus indentation load relationship for the interacting model is illustrated in Fig. 3. This is similar in behavior to that of various types of polycrystalline ceramics showing the so-called 'microstructural R-curve'.[3,4] The dashed line in Fig. 3 shows the experimental relation for the non-interacting model which was plotted in Fig. 2. It is evident that the transition behavior from the c- to the c_0-regimes occurs asymptotically because of the strong interaction between c and c_0. At the upper extremes of the indentation load the strength is determined by the central flaw (c), while at the low extremes of the indentation load the strength is determined by the model inherent flaws (c_0).

Examples of micrographs of the indentation flaws for the non-interacting ($P = 4{\cdot}9$ N, $P_0 = 4{\cdot}9$ N, $r = 300\,\mu$m) and the interacting models ($P = 4{\cdot}9$ N, $P_0 = 4{\cdot}9$ N, $r = 150\,\mu$m) are shown in Fig. 4(a) and (b), respectively. Figure 4(b) illustrates a typical example for a strong interaction between c and c_0.

4 Discussion

4.1 The dependence of apparent fracture toughness on flaw size

The strength (σ) versus indentation load (P) relationships of Figs 2 and 3 can be converted into the strength (σ) versus flaw size (c) relations in Figs 5 and 6 using the size of the 'central' flaw (c). The σ–c relationships in the larger flaw region ($c > c_0$) are well described experimentally by

$$\sigma = K_c/0{\cdot}64(\pi c)^{1/2} \quad (3)$$

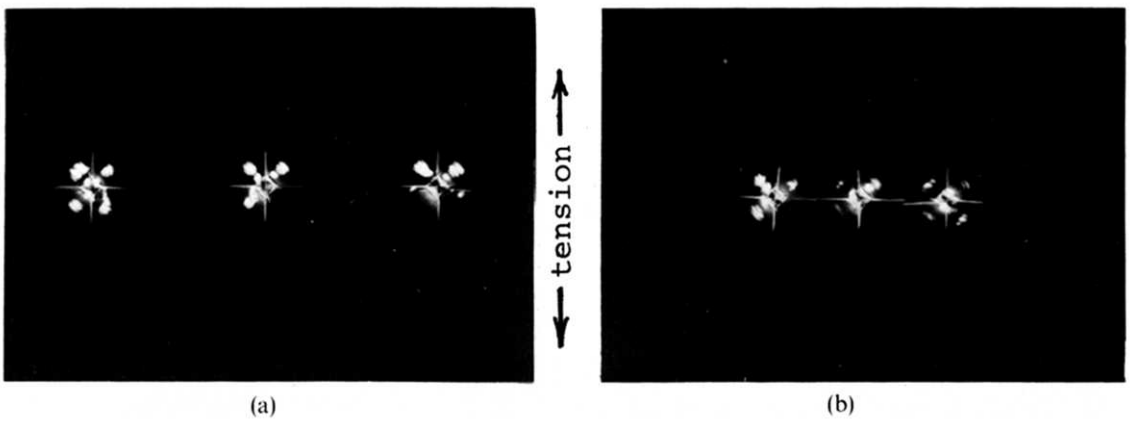

Fig. 4. Optical observations of indentation-induced flaws (c and c_0) for (a) the non-interacting model ($P = 4{\cdot}9$ N, $P_0 = 4{\cdot}9$ N, $r = 300\,\mu$m) and (b) the interacting model ($P = 4{\cdot}9$ N, $P_0 = 4{\cdot}9$ N, $r = 150\,\mu$m).

both for the non-interacting and the interacting models, where the K_c value was assumed to be 0·8 MPam$^{1/2}$ for soda-lime glass. Note that the experimentally determined factor, 0·64, in eqn (3) coincides with the numerical prediction by Newman & Raju,[6] and Ishida *et al.*,[7] which has been shown in eqn (2). This coincidence in the numerical factor after assuming the reasonable toughness value of 0·8 MPam$^{1/2}$ for soda-lime glass recognizes that the contact residual stress introduced by indentation is relieved by immersing the test specimens into water for 24 h as described in the preceding section, and is so small as to neglect the effect on the measured fracture toughness.

When the size of the central flaw (c) approaches that of the model inherent flaws (c_0), the well-defined transition in the strength is seen.

The dependence of the apparent fracture toughness ($K_c^{app}(c)$) on the size of central flaw (c) is plotted in Figs 7 and 8 for the non-interacting and the interacting models, respectively. The $K_c^{app}(c)$ value was calculated by eqn (2) using the flexural strength (σ) and the central flaw size (c). As would be expected from the K_c^{app} relationships in Figs 7 and 8, both the non-interacting and the interacting models yield a well-defined $c^{1/2}$ behaviour in the region of $c/c_0 < 1$. This is a similar type of behavior to that which has been reported for a number of polycrystalline ceramics, and has been termed 'microstructural R-curve'.[3,4] The microstructural interaction between the strength-controlling flaw and the polycrystalline ceramic microstructure has been used to theorize on this R-curve behavior.[3] In the present model fracture tests, however, the $c^{1/2}$ behavior in the apparent toughness is not caused by the microstructural interaction, but rather by the scaling transition of the fracture origin from the strength-controlling central flaw (c) to the inherent flaw (c_0). It is the flaw–flaw interaction that controls the transition behavior, such as sharp or asymptotic transition, between the $c^{1/2}$ proportional and the toughness plateau regions in the relationship of K_c^{app} versus c. The sharp transition for the non-interacting model (Fig. 7) and the asymptotic transition for the interacting model (Fig. 8) actually demonstrate the difference in this flaw–flaw interaction.

Given the homogeneous and continuous nature of the soda-lime glass, microstructural R-curve

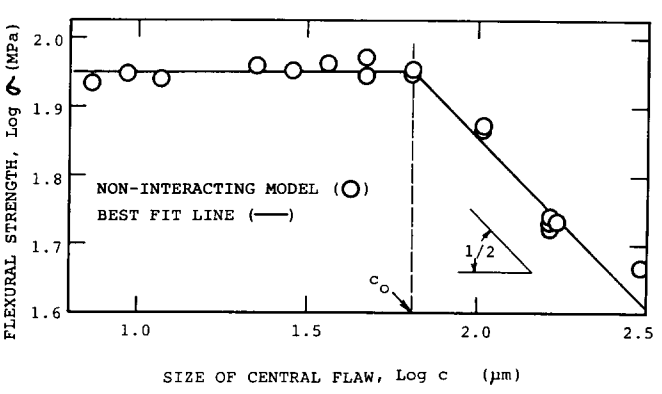

Fig. 5. Flexural strength of the non-interacting model as a function of the size of central flaw (c).

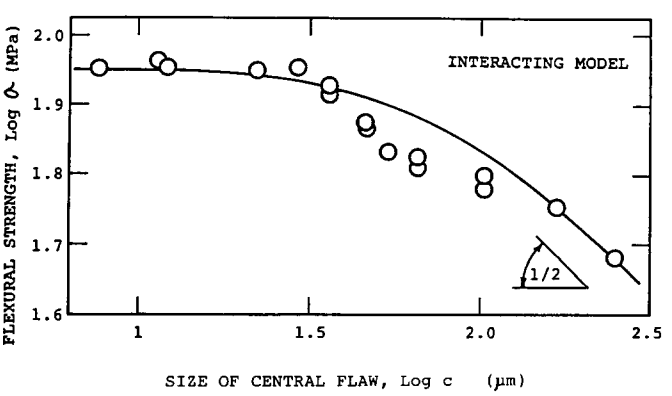

Fig. 6. Dependence of the flexural strength of the interacting model on the size of central flaw (c). Solid curve was calculated using eqns (6) and (7) with $\Phi = 0{\cdot}64$, $K_c = 0{\cdot}8$ MPam$^{1/2}$, $c_0 = 65\,\mu$m and $I(c/c_0) = \exp[-(c/c_0)]$.

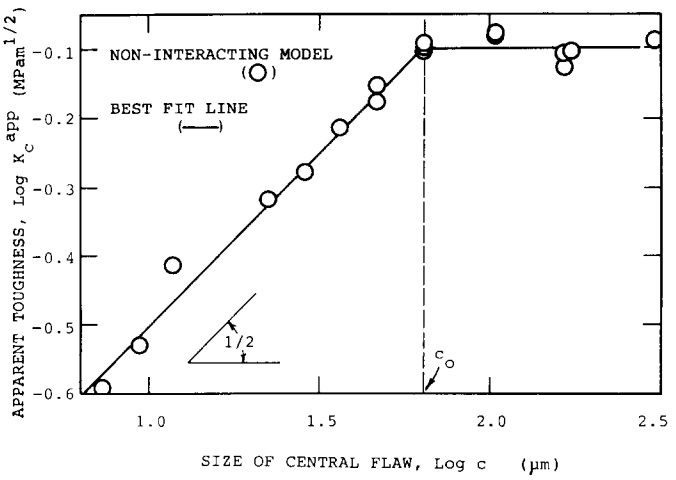

Fig. 7. Apparent toughness of the non-interacting model as a function of the size of central flaw (c).

behavior is unlikely, since soda-lime glass has a constant toughness value of about 0·8 MPam$^{1/2}$ which must be independent of flaw size in the mm- to μm-regions. Such a unique $c^{1/2}$ behavior in soda-lime glass is obviously derived from the 'apparent' fracture toughness approach, where the change in the strength which is associated with the scaling transition of the fracture origin is simply 'assumed' to correspond to the change in the 'apparent' fracture toughness, and the strength is always considered to be dominated by the strength-controlling central flaw (c) even in the region of $c \ll c_0$.[3,4]

The transition of the fracture origin from strength-controlling to inherent flaws in usual polycrystalline ceramics is very difficult if not impossible to distinguish. In the present model fracture tests, however, the use of homogeneous glass and well-defined flaws has made it quite easy to demonstrate that $c^{1/2}$ behavior in relation of K_c^{app}

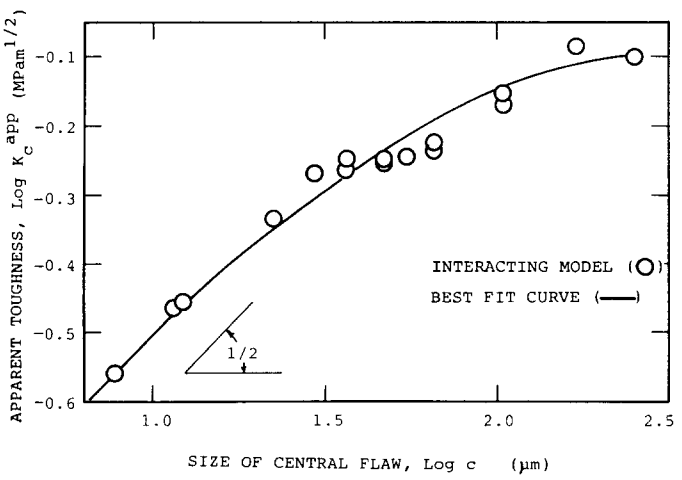

Fig. 8. Dependence of the apparent toughness of interacting model on the size of central flaw (c).

versus c arises from the transition of the fracture origin, and not from the change in the fracture toughness.

4.2 Strength–flaw size relationship and scaling transition of the fracture origin

Phenomenologically possible expressions which unify the σ–c relationship over a wide range of flaw size might be developed by combining the two extreme strength–flaw size relations:

$$\sigma = K_c/[\Phi(\pi c)^{1/2}] \tag{4}$$

for $c/c_0 \gg 1$, and

$$\sigma = K_c/[\Phi(\pi c_0)^{1/2}] \tag{5}$$

for $c/c_0 \ll 1$, where Φ stands for the shape factor of the microflaws. Considering the difference in transition behavior between the non-interacting and the interacting models as illustrated in Figs 5 and 6,

$$\sigma = K_c/\Phi[\pi(c + \tilde{c}_0)]^{1/2} \tag{6}$$

The characteristic flaw size, $\tilde{c}_0$, is defined by

$$\tilde{c}_0 = I(c/c_0) \cdot c_0 \tag{7}$$

using the inherent flaw size (c_0). In eqn (7), the microstructural interaction function, $I(c/c_0)$, which reflects the detailed information of the microstructural interaction between the strength-controlling (c) and inherent (c_0) flaws, is a dimensionless function varying from 0 (for $c/c_0 \gg 1$) to 1 (for $c/c_0 \ll 1$). Equation (6) satisfies both the extreme expressions of eqns (4) and (5), for $c/c_0 \gg 1$ and $\ll 1$, respectively, as well as describing the transition behavior from the $c^{1/2}$ to the strength plateau regions in the σ–c relationship as dictated by the interaction function, $I(c/c_0)$. For example, the sharp transition, as observed in the non-interacting model, is represented quantitatively by eqn (6) with eqn (7) using $\Phi = 0{\cdot}64$, $K_c = 0{\cdot}80$ MPam$^{1/2}$, and the microstructural interaction function:

$$I(c/c_0) = (1 - c/c_0) \cdot H(1 - c/c_0) \tag{8}$$

where $H(x)$ stands for the Heaviside step function, giving 0 for $x < 0$ and 1 for $x \geq 0$.

The authors have no information on the functional form of $I(c/c_0)$ for the general case of the microstructural interaction. However, the empirical determination of the $I(c/c_0)$ function and the insight of its physical significance aids the understanding of the essential role of the microstructural interaction in the relationship of strength versus flaw size. Through an example, as depicted in Fig. 6 by a solid curve, the observed behavior of the interacting

model can be well-expressed using the following exponential form of the $I(c/c_0)$ function;

$$I(c/c_0) = \exp[-(c/c_0)] \quad (9)$$

and $\Phi = 0{\cdot}64$, $K_c = 0{\cdot}80\,\mathrm{MPam}^{1/2}$, although the physical meaning of the exponential interaction is unknown. The application of the concept of this interaction function to real polycrystalline ceramics has been conducted by the present authors.[8]

5 Conclusions

The microstructural scaling transition of fracture origin was suggested to be one of the possible implications as recognized through the distinctive strength plateau of polycrystalline ceramics which occurs as the strength-controlling crack size decreases to its characteristic value. Model fracture tests using defect-free float glass demonstrated two different types of transition, i.e. sharp and asymptotic transitions, in the strength–flaw size relationship, reflecting the difference in the manner of flaw–flaw interaction between the indented model flaws.

Phenomenological expressions based on the microstructural scaling transition of fracture origin were developed to describe the strength–flaw size relationship over a wide range of flaw dimensions. The microstructural interaction function, $I(c/c_0)$, involving the detailed information on the microstructural interaction, was found to be the most significant parameter for evaluating the strength–flaw size relationship. Future experimental studies of the $I(c/c_0)$ function for various kinds of polycrystalline ceramics with a wide variety of microstructures would provide an essential understanding of the role of grain boundaries in the strengths of brittle materials.

Acknowledgement

This work was completed with support from the Japan Ministry of Education under a Grant-in-Aid for Scientific Research (No. 01550598).

References

1. Rice, R. W., Freiman, S. W. & Mecholsky, Jr, J. J., The dependence of strength-controlling fracture energy on the flaw size to grain size ratio. *J. Am. Ceram. Soc.*, **63** (1980) 129–36.
2. Rice, R. W., Specimen size–tensile strength relations for a hot-pressed alumina and lead zirconate/titanate. *Am. Ceram. Soc.*, **66** (1987) 794–8.
3. Cook, R. F., Lawn, B. R. & Fairbanks, C. J., Microstructure–strength properties in ceramics: I. Effect of crack size on toughness. *J. Am. Ceram. Soc.*, **68** (1985) 604–15.
4. Usami, S., Kimoto, H., Takahashi, I. & Shida, S., Strength of ceramic materials containing small flaws. *Eng. Fract. Mech.*, **23** (1986) 745–61.
5. Timoshenko, S., *Strength of Materials*, Parts I and II. D. Van Nostrand, New Jersey, 1976.
6. Newman, J. C. & Raju, I. S., An empirical stress intensity factor equation for the surface crack. *Eng. Fract. Mech.*, **15** (1981) 185–92.
7. Ishida, M., Noguchi, H. & Yoshida, T., Tension and bending of finite thickness plates with a semi-elliptical surface crack. *Int. J. Fract.*, **26** (1984) 157–88.
8. Miyajima, T. & Sakai, M., An application of indentation method to the fracture mechanics study of a polycrystalline graphite. *J. Mater. Sci.* (in press).